

EXAFS indication of double-well potential for oxygen vibration in  $\text{Ba}_{1-x}\text{K}_x\text{BiO}_3$ 

A. P. Menushenkov and K. V. Klementev

*Moscow State Engineering Physics Institute, 115409 Moscow, Russia*

(November 23, 2018)

X-ray absorption spectra of oxide systems  $\text{Ba}_{1-x}\text{K}_x\text{BiO}_3$  and  $\text{BaPbO}_3$  above Bi- and Pb- $L_3$  absorption edges were investigated. It was shown that oxygen ions move in double-well potential and their oscillations are correlated with charge carrier movement. Observed breathing-like oxygen vibration in double-well potential with large amplitude and low frequency causes the strong electron-phonon coupling and high  $T_c$  values in doped  $\text{BaBiO}_3$ . Based on the experimental data, the model of relationship of electronic and local crystal structures is proposed that is in a good agreement with the results of transport measurements, inelastic neutron and electron scattering, Raman scattering, and photoemission spectroscopy. In the framework of the model the possible reasons of superconductivity in perovskite-like oxides are discussed.

61.10.Ht, 74.72.Yg, 78.70.Dm

## I. INTRODUCTION

Though superconductivity in  $\text{BaPb}_{1-x}\text{Bi}_x\text{O}_3$  (BPBO) was discovered significantly earlier [1] than in cuprates, the question of the nature of superconducting state in this oxide as well as in cognate system  $\text{Ba}_{1-x}\text{K}_x\text{BiO}_3$  (BKBO) is still unsolved.

The structures of crystal lattice of copper oxide high temperature superconductors (HTSC's) and bismuth-based oxides have some important common characteristics. The both oxide classes have perovskite-like lattice with  $\text{CuO}_n$  ( $n=4, 5, 6$ ) or  $\text{Bi(Pb)O}_6$  complexes joined by the common oxygen ions. In bismuthates, the intersection of octahedral complexes in the three crystallographic directions determines their three-dimensional cubic structure. The  $\text{CuO}_n$  complexes are joined in  $\text{CuO}_2$  planes, which makes the two-dimensional structure of copper-oxides.

Because of strong hybridisation of covalent  $\text{Bi(Pb)}6s$ ,  $\text{Cu}3d - \text{O}2p_\sigma$  bonds, the above mentioned complexes are the most tightly bound items of the perovskite-like structure. Therefore such important peculiarities of perovskite structure as lattice instability in respect to soft tilting mode of  $\text{CuO}_n$  or  $\text{BiO}_6$  complexes (see for review [2]) and highly anisotropic thermal factors of oxygen ions vibration [3], which point out the large amplitude of rotation oscillations, are inherent to the both classes of superconducting oxides and cause anharmonic vibrations of oxygen atoms that may be described by movement in a double-well potential [4,5]. These structural instabilities of perovskite-like lattice can be related with the transition to superconducting state [4,5,2].

The layered structure of copper oxide compounds, presence of several non-equivalent copper positions, and a number of different Cu-O bonds complicate the local structure analysis. At the same time, the simplicity of cubic three-dimensional structure of BPBO-BKBO systems makes the interpretation of experimental data easier to a great extent. Relatively low temperatures of superconducting transition  $T_c \simeq 13\text{ K}$  in  $\text{BaPb}_{0.75}\text{Bi}_{0.25}\text{O}_3$  [1]

and  $T_c \simeq 30\text{ K}$  in  $\text{Ba}_{0.6}\text{K}_{0.4}\text{BiO}_3$  [6], the values of superconducting gap  $2\Delta(0)/kT_c = 3.6 \pm 0.1$  for BPBO [7] and  $2\Delta(0)/kT_c = 3.5 \pm 0.5$  for BKBO [8], and a sizeable oxygen isotope effect [9] allow one to rely on standard BCS-theory of superconductivity, not excluding a possible realisation of other mechanisms. The simpler electronic structure of  $s-p$  valence band of BPBO-BKBO systems in comparison with  $d-p$  band of cuprates favours the establishment of relationship of crystal and electronic structures in these compounds.

However, even for these relatively simple systems there is no agreement so far on a number of crucial aspects: crystal structure symmetry and lattice dynamics [10,11], electronic structure [12], bismuth valence state [13–16]. The most part of unusual properties of  $\text{BaBiO}_3$ -family compounds mentioned in early review [17] are still unexplained.

In addition, the average structural data contradicts the local ones. Integral crystallographic methods point to the simple cubic lattice in BKBO ( $x > 0.37$ ) [11]. In contrast to this, the EXAFS-analysis of four nearest spheres of bismuth environment [30] reveals a local tilting of octahedra by  $4-5^\circ$ , and Raman spectra evidence for a local lowering of symmetry from simple cubic [31].

EXAFS-analysis of the nearest oxygen octahedral environment of Bi in metallic BKBO compound with  $x = 0.4$  previously was made in harmonic approach [32,33] and pointed out at least one unresolved problem. Temperature dependence of Debye-Waller factor  $\sigma^2(T)$  found by Heald *et al.* [32] can be described in Einstein approximation, which is suitable for harmonic systems, only if one takes into account the temperature independent factor of  $0.0025 \text{ \AA}^2$ . The attempt to explain this fact due to some static disorder with doping was denied since  $\sigma^2(T)$  of the next Bi-Ba and Bi-Bi shells show the absence of any disorder. Similar weakly varying  $\sigma^2(T)$  dependence was found in [33]. Thus, it was observed that amplitude of low temperature Bi-O vibrations in metallic BKBO compound with  $x = 0.4$  is too high (more than twice larger than in metallic  $\text{BaPbO}_3$  compound) [22,34].

Besides, our careful measurements [34] of temperature dependent EXAFS-spectra of undoped BaBiO<sub>3</sub> which were also treated in harmonic approach showed absolutely abnormal increasing of  $\sigma^2$  values of both Bi-O bonds with temperature decreasing from 90 K. We explained these anomalies by the influence of anharmonic rotational vibrations of oxygen octahedra which become pronounced at low temperatures [29], the model of connection of superconductivity with rotation mode asymmetry was proposed [35].

The above contradictions in description for local structure lead us to necessity of EXAFS analysis of the nearest Bi-O shell in anharmonic approach.

In the present paper we report the results of temperature dependent EXAFS-investigation of BPBO-BKBO systems firstly treated in anharmonic approach based on the idea of such an analysis for apical oxygen atoms in YBa<sub>2</sub>Cu<sub>3</sub>O<sub>7- $\delta$</sub>  proposed by J. Mustre de Leon *et al.* [36] We have analysed EXAFS function  $\chi(k)$ , using the new program “VIPER for Windows” [37], by construction of the model potentials of atomic vibrations, subsequent calculation of the pair radial distribution function, and calculation of the model  $\chi(k)$ . This new approach for the EXAFS-analysis of Bi-based oxides gives us an opportunity to investigate the character of oxygen atom vibrations and, in combination with our previous local electronic structure studies by XANES (x-ray absorption near edge structure) spectroscopy [38], to understand the nature of the structural phase transitions in these systems and to explain practically all above contradictions.

In Sec. II we describe the experimental details and present the procedure of data treatment. The general results are given in Sec. III. In Sec. IV we relate the local crystal structure with local electronic structure, which is the base of our processing of experimental data. In Sec. V we discuss the possible superconductive mechanism and demonstrate how the oscillations of oxygen atoms in double-well potential contributes to superconductivity in BKBO.

## II. EXPERIMENTAL AND DATA ANALYSIS

In this work we have investigated ceramic samples of BaPbO<sub>3</sub> and BKBO with  $x = 0, 0.4, 0.5$  synthesised as described in [39]. The materials were examined by x-ray powder diffraction for phase purity. The samples were controlled by transport and susceptibility measurements. BaBiO<sub>3</sub> showed semiconductor-like behaviour, the compositions BKBO with  $x = 0.4$  and  $0.5$  showed typical metallic  $\rho(T)$  dependence and superconducting properties with  $T_c \simeq 30$  K and  $T_c \simeq 16$  K, correspondingly. BaPbO<sub>3</sub> samples were metallic but not superconducting at all temperatures.

For the XAS measurements, a crushed fine powder was precipitated onto a micropore substrate. The thickness of samples was about two absorption lengths at the chosen

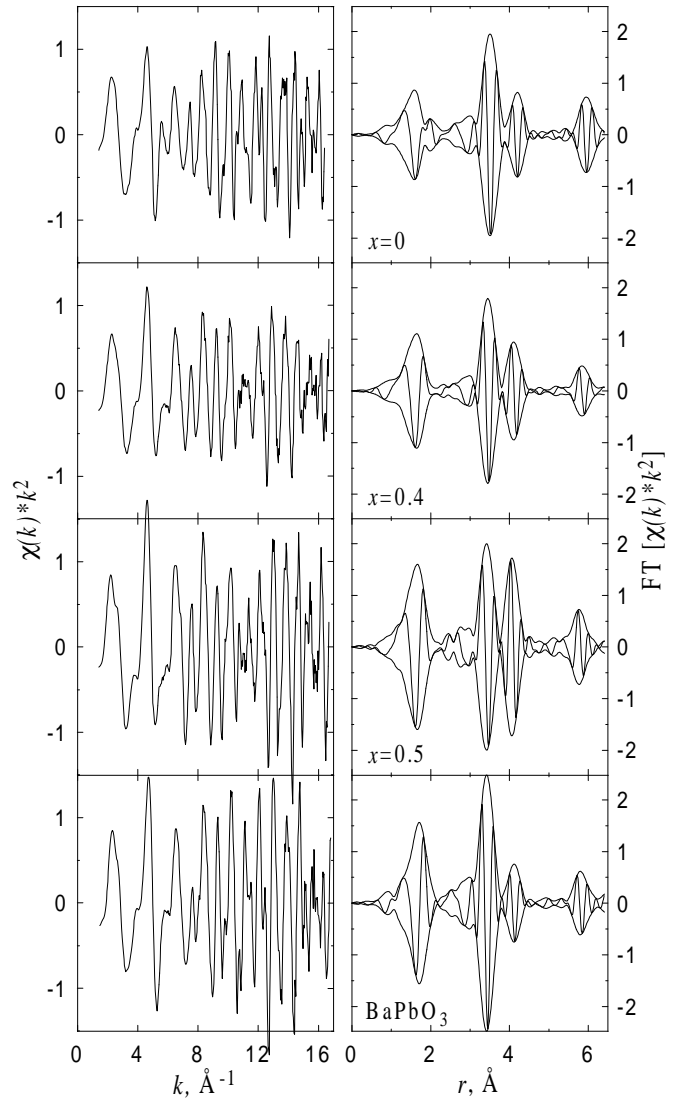


FIG. 1. Experimental EXAFS  $\chi(k)k^2$  (left) and its Fourier transform magnitude and imaginary part (right) for Ba<sub>1-x</sub>K<sub>x</sub>BiO<sub>3</sub> ( $x = 0, 0.4, 0.5$ ) and BaPbO<sub>3</sub> at 7 K.

absorption edge.

The x-ray absorption spectra were collected at D-21 line (XAS-13) of DCI (LURE, Orsay, France) synchrotron operated at energy 1.85 GeV and the average current  $\sim 250$  mA of positron beam at the  $L_3$  edges of Bi (13040.6 eV) and Pb (13426 eV). Energy resolution of the double-crystal Si [311] monochromator (detuned to reject 50% of the incident signal in order to minimise harmonic contamination) with a 0.4 mm slit at 13 keV was about 2–3 eV. The low temperature measurements were carried out using a liquid helium circulation type cryostat with a temperature control of  $\pm 1$  K.

The background in the experimental spectra was removed as described in [40], taking care to remove the low frequency oscillations. EXAFS-functions  $\chi(k)k^2$  ob-

tained from absorption spectra were Fourier transformed in the wave number range  $k$  from 1.5 to  $16.5 \text{ \AA}^{-1}$ , using Kaiser-Bessel windowing function. Back Fourier transform was done using a Hanning window from  $\sim 1$  to  $\sim 2 \text{ \AA}$  corresponding to the first Bi-O near-neighbour shell. In such a case, the number of independent experimental points [42] was  $N_{exp} = 2\Delta k \Delta r / \pi + 2 \approx 11$ .

The model EXAFS-function for pair atomic absorber-scatterer oscillations is constructed as follows. Suppose we know the potential of these oscillations as a parametric function of interatomic distance. Solving the stationary Schrödinger equation for the particle with reduced mass of the atomic pair [37], one obtains a pair radial distribution function (PRDF) of atoms in  $i$ -th sphere:

$$g_i(r) = N_i \sum_n |\Psi_n(r)|^2 e^{-E_n/kT} / \sum_n e^{-E_n/kT}, \quad (1)$$

where  $N_i$  is the coordination number,  $E_n$  and  $\Psi_n$  are  $n$ -th energy level and its corresponding wave function. Given PRDF's, the model EXAFS function calculated as

$$\chi(k) = \frac{1}{k} \sum_i F_i(k) \int_{r_{min}}^{r_{max}} g_i(r) \sin[2kr + \phi_i(k)] / r^2 dr, \quad (2)$$

where  $k = \sqrt{2m_e/\hbar^2(E - E_{th})}$  is the photoelectron wave number referenced to the ionisation threshold  $E_{th}$ ,  $r_{min}$  and  $r_{max}$  are determined by the windowing function of back Fourier transform. The phase shift  $\phi_i(k)$  and scattering amplitude  $F_i(k)$  were calculated using FEFF-6 code [43] for six-shell cluster with crystallographic data from neutron diffraction study [11] and using default set of the FEFF-6 parameters. The potential parameters were extracted from the model-to-experimental EXAFS-function fits.

### III. GENERAL RESULTS

In Fig. 1 (left) we show the experimental  $\chi(k)k^2$  for BKBO  $x=0, 0.4, 0.5$  and for BaPbO<sub>3</sub> measured at  $L_3$  Bi(Pb) absorption edge at 7 K. Good signal-to-noise ratio seen even for maximal wave number values  $k \gtrsim 16 \text{ \AA}^{-1}$  indicates the high spectra quality. The absence of signal on the Fourier transform in the low- $r$  range Fig. 1 (right) testifies for correct background removal procedure.

#### A. BaBiO<sub>3</sub>

EXAFS-researches [21,22] of BaBiO<sub>3</sub> confirm the results of crystallographic works [13,10,11]. According to them, there exist two inequivalent bismuth positions characterised by two Bi-O bond lengths. The equality of coordination numbers of the two BiO<sub>6</sub> spheres points out that the BaBiO<sub>3</sub> structure represents the ordered alternation of small and large BiO<sub>6</sub> octahedra in barium

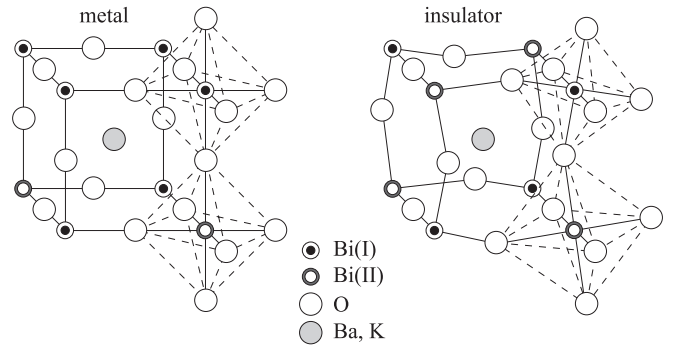


FIG. 2. Sketch of crystal structure of Ba<sub>1-x</sub>K<sub>x</sub>BiO<sub>3</sub> in metallic ( $x > 0.37$ ) and insulating ( $x < 0.37$ ) states.

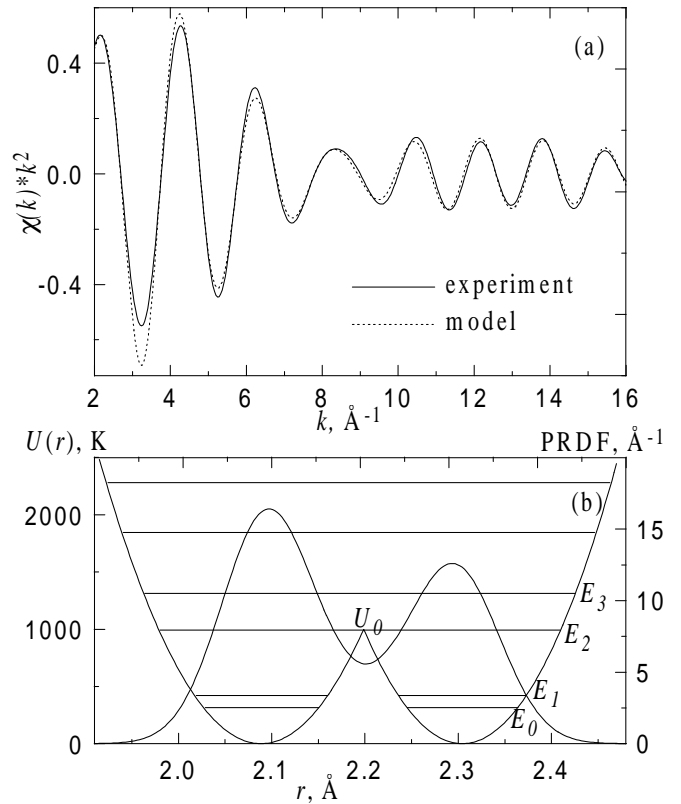


FIG. 3. Experimental and model  $\chi(k)k^2$  EXAFS for BaBiO<sub>3</sub> at 7 K for the first Bi-O near-neighbour shell (a) and the model potential with corresponding PRDF and energy levels (b).  $U_0$  is the energy of potential barrier

lattice. Such an alternation together with static rotation distortion around  $[110]$  axis produce the monoclinic distortion of cubic lattice [13,10,11] (Fig. 2). As will be shown in Sec. IV, to the larger soft octahedra corresponds the configuration BiO<sub>6</sub>, and to the smaller rigid octahedra corresponds Bi $\underline{L}^2$ O<sub>6</sub>. Here,  $\underline{L}^2$  denotes the hole pair in antibonding Bi $6s$ O $2p_{\sigma^*}$  orbital of the octahedral complex.

In Fig. 3(a) the experimental  $\chi(k)k^2$  EXAFS for BaBiO<sub>3</sub> at 7 K for the first Bi-O near-neighbour shell is shown. The pronounced beating near 8 Å<sup>-1</sup> evidences for existence of at least two different lengths of Bi-O bonds. In all previous EXAFS-researches [21,22,32–34] the EXAFS-function was quite successfully fitted in harmonic approximation as a sum of two independent harmonic functions with different bond lengths and Debye-Waller factors. However, temperature dependencies of Debye-Waller factors contradict to the harmonic Einstein model [34]. This argues against the independence of oxygen atom vibrations in two neighbouring octahedra.

In this work, we model the oscillatory Bi-O potential as follows. Inequivalence of the two types of BiO<sub>6</sub> octahedra is due to presence or absence of a hole pair in the hybridised molecular orbitals Bi6sO2p<sub>σ</sub>\* (see Sec. IV). Suppose, the movement of oxygen atoms may transfer a hole pair from one octahedron to another. Such a movement exchanges the roles of two inequivalent octahedra and requires a double-well form of oscillatory Bi-O potential. Here, we take a parabolic form of each well  $U_1 = \kappa_1(r - r_1)^2/2$  and  $U_2 = \kappa_2(r - r_2)^2/2$  which are joined continuously. Given the calculated  $\chi(k)$ , defined by Eqs. (1) and (2), we perform a least-squares fit between the model and experimental  $\chi(k)$  over the range  $k = 2\text{--}16\text{ Å}^{-1}$  (see Fig. 3(a)). The six parameters determined by the fit were  $E_{th}$ ,  $r_1$ ,  $r_2$ ,  $\kappa_1$ ,  $\kappa_2$ , and  $N$ . The number of parameters here is the same as for fitting in the harmonic approximation.

The analysis of parameters of double-well potential allows one to draw the following conclusions on the oscillations of oxygen atoms in BaBiO<sub>3</sub>. (i) At low temperatures there exist two explicit peaks on PRDF, that is why x-ray and neutron diffraction detect the static distortions in BaBiO<sub>3</sub>. (ii) Even at low temperatures, the tunnelling probability between the two wells is non-zero. As it will be discussed in Sec. IV, such a tunnelling is equivalent to the dynamic exchange  $\text{Bi}\bar{\text{L}}^2\text{O}_6 \leftrightarrow \text{BiO}_6$  and explains observed activation conductivity in BaBiO<sub>3</sub>. (iii) The temperature rise leads to gradual increase of probability of interwell tunnelling and to the structural transition to cubic phase found at 750–800 K [13]. (iv) Non-equidistance of energy levels implies that oscillations of breathing- or stretching types with several frequencies exist:  $\omega_0 = E_1 - E_0$ ,  $\omega_1 = E_2 - E_0$ ,  $\omega_2 = E_3 - E_0$ , etc. The latter are gradually manifested at high temperatures. (v) The positions of minima of double-well potential in our model are the *average* positions. They are spaced widely at maximal octahedra tilting and spaced closely at minimal octahedra tilting. In the latter case the probability of interwell tunnelling is maximal. In this sense the tunnelling frequency  $\omega_0$  is bounded by soft rotation mode frequency.

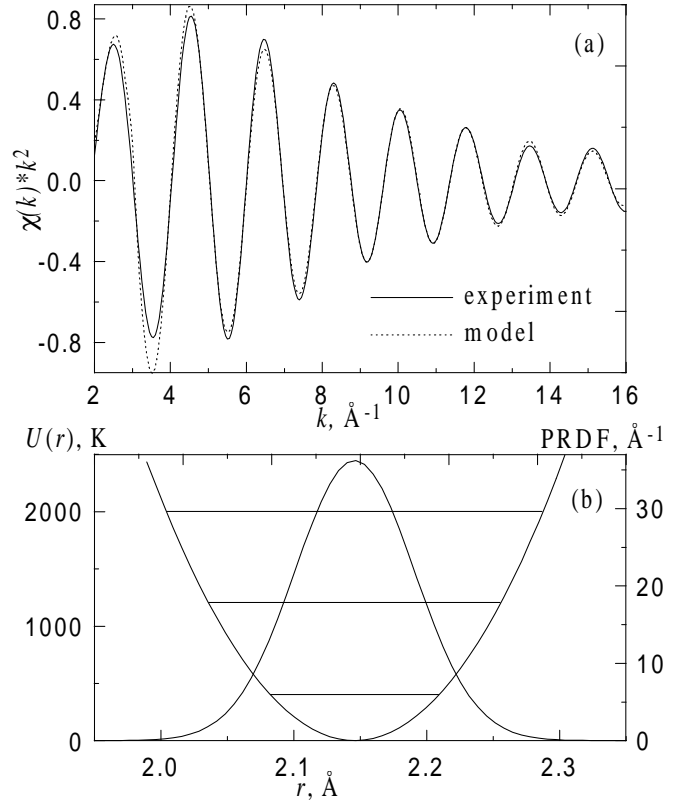


FIG. 4. Experimental and model  $\chi(k)k^2$  EXAFS for BaPbO<sub>3</sub> at 7 K for the first Pb-O near-neighbour shell (a) and the model potential with corresponding PRDF and energy levels (b).

## B. BaPbO<sub>3</sub>

The experimental  $\chi(k)k^2$  EXAFS for BaPbO<sub>3</sub> for the first Pb-O near-neighbour shell at all temperatures represents a sinusoid with no beatings and phase breaks (Fig. 4) and fitted well, using a single parabolic potential. This means that all Pb-O bonds in BaPbO<sub>3</sub> are equivalent and the breathing-type distortion is absent.

## C. Ba<sub>1-x</sub>K<sub>x</sub>BiO<sub>3</sub>

The experimental  $\chi(k)k^2$  EXAFS function for BKBO ( $x = 0.4$ ) at 7 K for the first Bi-O near-neighbour shell is shown in Fig. 5(a), solid curve. Also, the model calculated in harmonic approach (as in [32,33]) is shown as a dash-dot curve. It is seen that in the range  $k \gtrsim 12\text{ Å}^{-1}$  the harmonic approach fails. This argues for the anharmonic Bi-O vibration behaviour similar to BaBiO<sub>3</sub> case also in superconducting compositions BKBO. To a possible tendency in the cubic superconducting materials towards the same type of distortions as in BaBiO<sub>3</sub> was pointed earlier [32,44].

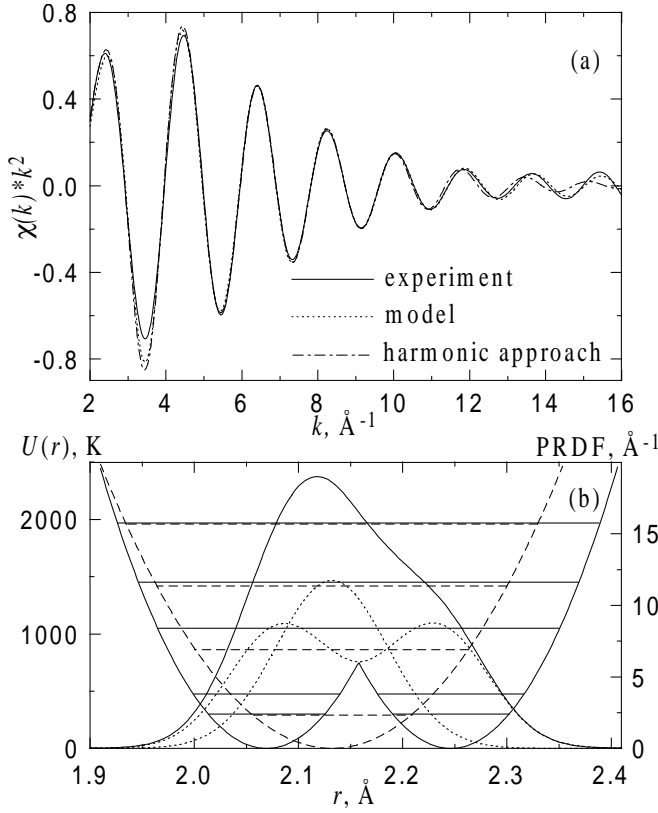


FIG. 5. Experimental and model  $\chi(k)k^2$  EXAFS for  $\text{Ba}_{0.6}\text{K}_{0.4}\text{BiO}_3$  at 7 K for the first Bi-O near-neighbour shell (a) and the model potentials (single-parabolic and double-parabolic) with corresponding PRDF's and energy levels (b). Total PRDF is shown by solid line.

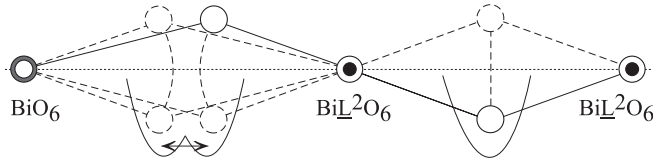


FIG. 6. The sketch of oxygen vibrations in  $\text{Ba}_{1-x}\text{K}_x\text{BiO}_3$  in the case of different (left) and equivalent (right) neighbouring octahedra with corresponding radial oscillatory potentials.

The K doping of  $\text{BaBiO}_3$  leads to partial replacement of the larger soft octahedra  $\text{BiO}_6$  by the smaller rigid octahedra  $\text{BiL}_2\text{O}_6$  (see details in Sec. IV). This causes a decrease and disappearance of static breathing and tilting distortions, but keeps the different rigidities of Bi-O bonds. Hence, the movement of an oxygen atom depends on that to which neighbouring octahedra this atom belongs. If the neighbouring octahedra are different, the oxygen atom oscillates in double-well potential as in  $\text{BaBiO}_3$ . If the octahedra are equal, the oxygen atom oscillates in single-parabolic potential as in  $\text{BaPbO}_3$  (see Fig. 6). The statistical weights of these two cases de-

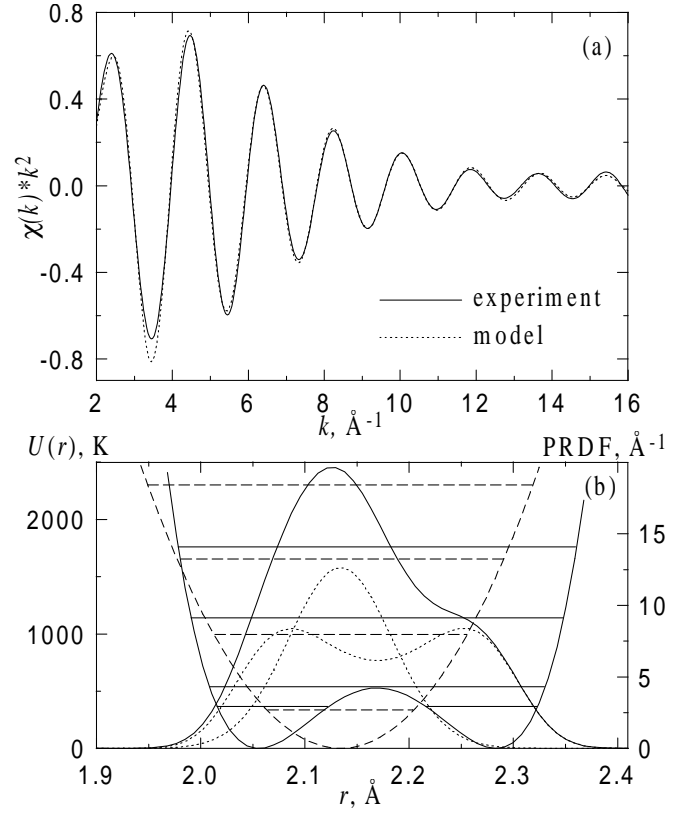


FIG. 7. Experimental and model  $\chi(k)k^2$  EXAFS for  $\text{Ba}_{0.6}\text{K}_{0.4}\text{BiO}_3$  at 7 K for the first Bi-O near-neighbour shell (a) and the model potentials (single-parabolic and polynomial of degree 4) with corresponding PRDF's and energy levels (b). Total PRDF is shown by solid line.

pend on the potassium content  $x$ , and are  $(1-x)$  and  $x$ , correspondingly. Here, the force constants of the two parabolas are assumed to be equal since their independent varying does not improve the fits, and the number of fitting parameters equals 7. The resulting model curve is presented in Fig. 5(a), dotted. It is seen from Fig. 5(b) that the total PRDF is unsplit, so it is not surprising that crystallographic measurements reveal the cubic structure [11] (e.g. at  $T = 10$  K  $a = 4.2742(1)$ ). Meanwhile, the first momentum of the radial distribution function derived from our model is in a good agreement with the diffraction data [11], which validates our calculated amplitudes and phases.

In this paragraph we address to the important question of statistical grounds for the choice among several possible models. Consider, first, the statistical chi-square function (labelled just like EXAFS-function, but this is the different value)

$$\chi^2 = \frac{N_{exp}}{M} \sum_i^M \left( \frac{\chi_{exp}(k_i) - \chi_{mod}(k_i)}{\varepsilon_i} \right)^2, \quad (3)$$

where  $M$  is the number of data points in the fit,  $N_{exp}$

TABLE I. Bi(Pb)-O parameters resulting from the fit to EXAFS data for BaPbO<sub>3</sub> and Ba<sub>1-x</sub>K<sub>x</sub>BiO<sub>3</sub> with  $x = 0, 0.4, 0.5$ .  $r$  and  $l$  are positions (Å) of potential minima and corresponding PRDF's first momenta,  $\kappa$  is the force constant (eV/Å<sup>2</sup>). The index 0 corresponds to parabolic potentials, the indices 1 and 2 correspond to the two parts of double-parabolic potentials.

BaPbO <sub>3</sub>			$x = 0$						$x = 0.4$						$x = 0.5$					
$T, K$	$r_0=l$	$\kappa_0$	$r_1$	$r_2$	$l_1$	$l_2$	$\kappa_1$	$\kappa_2$	$r_1$	$r_2$	$r_0$	$l$	$\kappa_{1,2}$	$\kappa_0$	$r_1$	$r_2$	$r_0$	$l$	$\kappa_{1,2}$	$\kappa_0$
7	2.15	24	2.08	2.30	2.09	2.285	11	9	2.07	2.245	2.13	2.145	17	9	2.065	2.20	2.11	2.12	38	20
10	2.15	17													2.07	2.20	2.12	2.125	27	11
20	2.155	15							2.07	2.235	2.13	2.14	28	18	2.05	2.20	2.12	2.125	36	16
30			2.09	2.305	2.095	2.295	15	14							2.06	2.195	2.12	2.125	33	17
40	2.145	11							2.07	2.24	2.12	2.145	28	18						
55			2.09	2.30	2.10	2.29	16	14	2.075	2.25	2.12	2.15	20	12	2.07	2.20	2.12	2.125	41	22
65			2.105	2.315	2.11	2.305	16	13	2.08	2.24	2.13	2.145	20	9	2.06	2.20	2.12	2.125	39	21
95	2.14	13	2.10	2.31	2.11	2.30	12	7							2.06	2.20	2.125	2.13	32	17
115			2.10	2.31	2.11	2.30	11	6	2.08	2.24	2.12	2.14	18	10						
135			2.105	2.31	2.11	2.30	13	5							2.07	2.20	2.12	2.125	33	16
195									2.08	2.24	2.12	2.145	20	11						
300	2.14	9	2.10	2.26	2.11	2.25	11	7	2.07	2.23	2.115	2.135	18	9	2.07	2.205	2.125	2.13	24	11

was introduced above,  $\varepsilon_i$  are the individual errors in the experimental data points. The latter were calculated as average of  $\sqrt{1/I_0 + 1/I_t}$ ,  $I_0$  and  $I_t$  being the intensities measured in the transmission EXAFS experiment. The  $\chi^2$  value must follow the  $\chi^2$  distribution law with degrees of freedom  $\nu = N_{exp} - P$ , where  $P$  is the number of parameters varied during the fit. That is  $\chi^2$  must be less than the critical value  $X_\nu^c$  of the  $\chi^2$  distribution with  $\nu$  degrees of freedom and the confidence level  $c$ . For our model in Fig. 5(a)  $\nu_2 = 11 - 7 = 4$  and  $\chi_2^2 = 5.3 < X_4^{0.95} = 9.5$ , but for single-Gaussian model  $\nu_1 = 11 - 4 = 7$  and  $\chi_1^2 = 16.8 > X_7^{0.95} = 14.1$ . Thus, our model meets the  $\chi^2$ -test while the simple harmonic model does not. It is quite natural that having increased the number of parameters we got decreased  $\chi^2$  value. But what the gain should be? The comparison between the two models can be performed on the basis of  $F$ -test. If the difference  $\chi_1^2 - \chi_2^2$  is physically meaningful, not due to presence of the noise, that is if the simpler model cannot describe some features in principle, this difference must *not* follow the  $\chi^2$  distribution law with  $\nu_1 - \nu_2$  degrees of freedom. Provided that  $\chi_2^2$  follows the  $\chi^2$  distribution with  $\nu_2$  degrees of freedom, the value  $F(\nu_1 - \nu_2, \nu_2) = (\chi_1^2/\chi_2^2 - 1)\nu_2/(\nu_1 - \nu_2)$  must not follow Fisher's  $F$ -distribution with  $\nu_1 - \nu_2$  and  $\nu_2$  degrees of freedom. That is  $F$  must be greater than the critical value  $F_{\nu_1 - \nu_2, \nu_2}^c$  of the  $F$  distribution with  $\nu_1 - \nu_2$  and  $\nu_2$  degrees of freedom and the confidence level  $c$ . Comparing the two models in Fig. 5(a), we find  $F(3, 4) = 2.89$ , which is equal to  $F_{3, 4}^{0.84}$ . Therefore, we can claim with 84% probability that we propose a better model than the simplest single-Gaussian.

The complete results for Bi(Pb) octahedral ( $N = 6$ ) oxygen environment in BaPbO<sub>3</sub> and Ba<sub>1-x</sub>K<sub>x</sub>BiO<sub>3</sub> with  $x = 0, 0.4, 0.5$  at various temperatures are listed in Table I. The uncertainties in the EXAFS distances and force constants are less than  $\pm 0.4\%$  and  $\pm 50\%$ , respec-

tively. (These increments cause an increase of less than 10% in the value of misfit.) It is seen from Figs. 3 and 5 that, in general, the positions of potential minima are not equal to the positions of PRDF's maxima. Because of that, among other parameters, we give the values of PRDF's centers of gravity, i.e. values that can be defined crystallographically. For BaBiO<sub>3</sub>, the centers of gravity were calculated for the two peaks of PRDF separately.

The parameters of potentials were obtained through the fit and, of course, depend on the form of the model potentials. To elucidate this influence, we constructed the model EXAFS function, using the polynomial of degree four:  $U = -\kappa(r - r_0)^2/2 + \xi(r - r_0)^4 + \kappa^2/(16\xi)$ , where the last term is introduced to zero the minimum values (Fig. 7). The number of fitting parameters here is the same as for double-parabolic potential. It turned out, that for the both potential forms the mean frequencies of Bi-O oscillations are practically identical for all temperatures. Because of this, in the present work we use double-parabolic potentials with parameters of clear meaning (potential minima positions and force constants) rather than a polynomial potential with abstract coefficients. Since the model EXAFS function weakly depends on the shape and value of interwell energy barrier  $U_0$ , we can not determine the  $U_0$  value from EXAFS measurements exactly.

It worth to notice that in the case of BaBiO<sub>3</sub> the above model of oxygen vibrations has some limitation due to the existence of the static rotation (tilting) distortion  $\sim 11^\circ$ . Thus, the distances observed from EXAFS spectra treatment are measured along Bi-O-Bi zigzag curve, but not along the Bi-Bi ([100]) direction as in BKBO. This may result in some difference between  $\kappa_1$  and  $\kappa_2$  values (see Fig. 3(b) and Table I) and some deviation of calculated frequency from real ones in BaBiO<sub>3</sub>.

## IV. RELATIONSHIP BETWEEN THE LOCAL CRYSTAL AND LOCAL ELECTRONIC STRUCTURES

### A. BaBiO<sub>3</sub>

The co-existence in BaBiO<sub>3</sub> of two different types of octahedra with two different Bi-O bond lengths and strengths reflects the different electronic structures of BiO<sub>6</sub> complexes.

Octahedral complexes represent the most tightly bound items of the perovskite-like structures because of strong covalence of Bi6s-O2p<sub>σ</sub> bonds. The valence band structure of BaBiO<sub>3</sub> is determined by overlapping of Bi6s and O2p orbitals [1,12], and, owing to strong Bi6s-O2p<sub>σ</sub> hybridisation, the octahedra can be considered as quasi-molecular complexes [49]. Each complex has ten electron levels consisting of a pair of bonding Bi6s-O2p<sub>σ</sub>, six nonbonding O2p<sub>π</sub>, and a pair of antibonding Bi6sO2p<sub>σ</sub>\* orbitals. A unit cell, which includes two octahedra, has 38 valence electrons (10 from two bismuth ions, 4 from two barium ions, and 24 from six oxygen atoms). However, the numbers of occupied states in the two octahedral complexes are different: octahedron BiL<sup>2</sup>O<sub>6</sub> carries 18 electrons and has one free level or a hole pair L<sup>2</sup> in the upper antibonding Bi6sO2p<sub>σ</sub>\* orbital, in octahedron BiO<sub>6</sub> with 20 electrons both antibonding orbitals are filled (Fig. 8). It is quite natural that BiL<sup>2</sup>O<sub>6</sub> octahedra have stiff (quasi-molecular) Bi-O bonds and the smaller radius, and BiO<sub>6</sub> octahedra represent non-stable molecules with filled antibonding orbitals and the larger radius. Because the sum of two nearest octahedra radii overcomes the lattice parameter *a*, the octahedral system must tilt around [110] axis, producing a monoclinic distortion in BaBiO<sub>3</sub> (see Fig. 2).

The assumption of equal electron filling for nearest octahedra (BiL<sup>1</sup>O<sub>6</sub>+BiL<sup>1</sup>O<sub>6</sub>) contradicts to experiments, since in this case equal Bi-O bond lengths and local magnetic ordering should be observed.

Therefore our new scheme of bismuth disproportionation 2BiL<sup>1</sup>O<sub>6</sub> → BiL<sup>2</sup>O<sub>6</sub>+BiO<sub>6</sub> is in full agreement with charge balance, presence of two types of octahedron complexes and absence of any local magnetic moment [47,48].

Because Ba<sup>2+</sup> in perovskite-type lattice is bound by pure ionic bond, the electron density is concentrated mainly in octahedra volume *V*<sub>0</sub> [27]. Hence, the energy of the highest occupied level *E*<sub>*f*</sub> is related to the octahedron radius *R* and the number of valence electrons *N* in a unit cell as

$$E_f \sim h^2 N^{2/3} / m_e V_0^{2/3} \sim h^2 N^{2/3} / m_e R^2, \quad (4)$$

where *h* is the Planck's constant, *m<sub>e</sub>* is the electron mass. This qualitative relation leaves out of account the deviation of Fermi surface from sphere [17]. Nevertheless, the value of *E<sub>f</sub>*, which transforms to the Fermi level *E<sub>F</sub>* at spatial overlapping of equal octahedra in the crystal, is

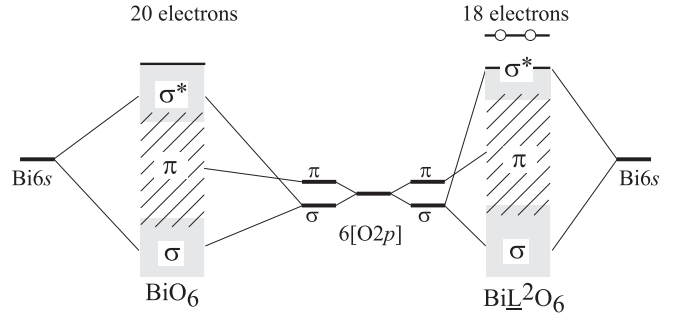


FIG. 8. The scheme of electronic structure formation for two different octahedral BiO<sub>6</sub> complexes.

in close connection with the octahedron radius and with the number of valence electrons.

According to expression (4), the local electronic structure is connected with the local crystal structure. In the left of Fig. 9(a), the case of hypothetical simple cubic structure of BaBiO<sub>3</sub> is shown. Real monoclinic structure arises from combined breathing (alternating octahedra with different radii *R*) and rotation distortions, which, according to (4), leads to the lowering of the energy *E<sub>f</sub>* of the highest occupied Bi6sO2p<sub>σ</sub>\* orbital in BiO<sub>6</sub> octahedron in comparison with energy *E<sub>h</sub>* of unoccupied Bi6sO2p<sub>σ</sub>\* orbital in BiL<sup>2</sup>O<sub>6</sub> octahedron. Hence, the repetitive sequence of empty level *E<sub>h</sub>* on the background of fully filled valence band represents the electronic structure of the ground state of BaBiO<sub>3</sub> (Fig. 9(a), right). In such a system there are no free carriers and conductivity occurs at hopping of carrier pair from one octahedron to another with the activation energy *E<sub>a</sub>* = *E<sub>h</sub>* − *E<sub>f</sub>*. In this process the movement of hole pair in real space leads to change of large octahedra to small ones and vice versa or to a dynamic exchange BiL<sup>2</sup>O<sub>6</sub> ↔ BiO<sub>6</sub>, in full accordance with vibrations in double-well potential showed in Fig. 3, and causes the hole-type conductivity. In this case, the activation energy *E<sub>a</sub>* means the pair localisation energy.

This picture agrees with results of investigation of temperature dependencies of conductivity and Hall coefficient:  $n(T) = n_0 \exp(-E'_a/k_B T)$  [17], where the value of hole concentration  $n_0 = 1.1 \times 10^{22} \text{ cm}^{-3}$  coincides with the concentration of unit cells, and the activation energy  $E'_a = 0.24 \text{ eV}$ , if one takes into account that in the case of two-particle activation conductivity, the number of hole pairs is equal to the number of BiL<sup>2</sup>O<sub>6</sub> complexes (concentration of which is half *n*<sub>0</sub>), and the activation energy  $E_a = 2E'_a = 0.48 \text{ eV}$ . It should be mentioned that the possibility of the two-particle (bipolaron) conductivity as a most probable mechanism of conductivity in BaBiO<sub>3</sub> was pointed to earlier [17].

Pair splitting and hopping of a single electron from one octahedron to another cost energy and lead to electronic structure reconstruction of the both octahedral complexes. Such a splitting can be achieved under optical excitation, which was observed experimentally as a photoconductivity peak at the photon energy  $h\nu = 1.9 \text{ eV}$

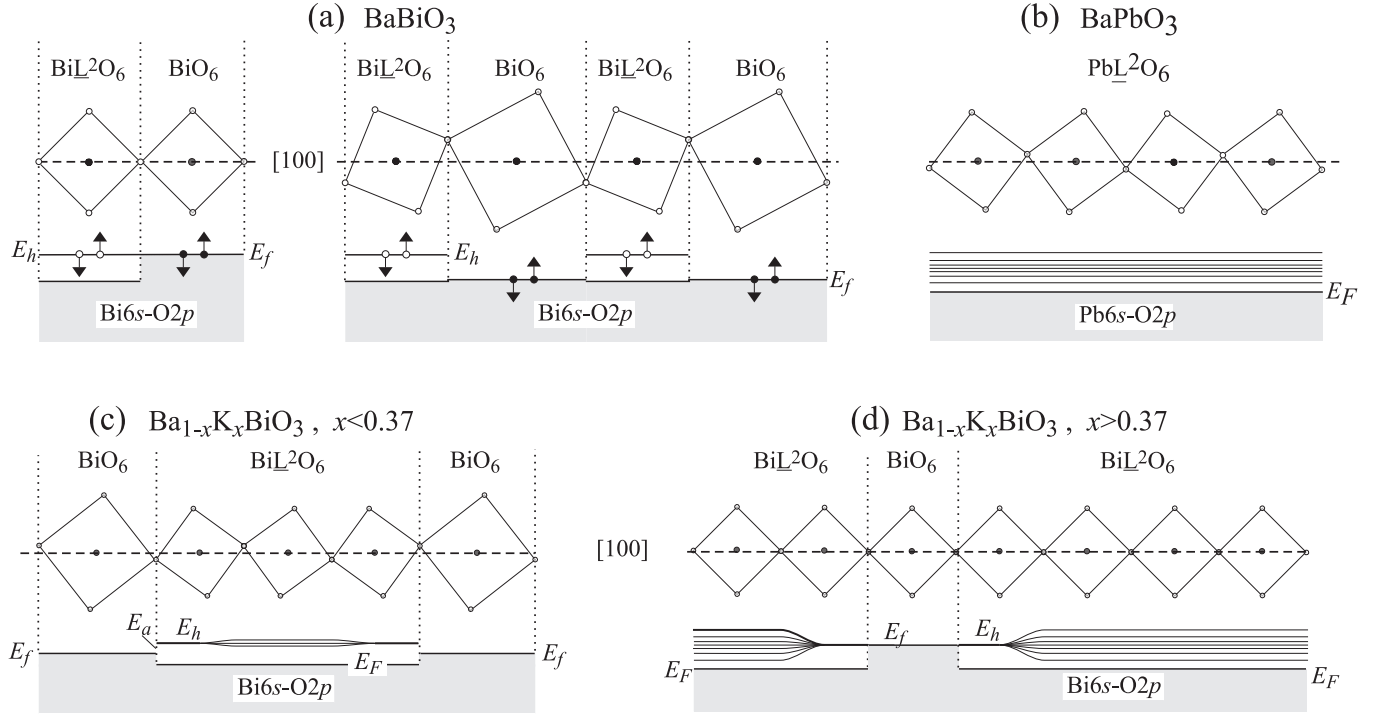


FIG. 9. The scheme of relationship between the local crystal and local electronic structures. (a) The ground state of BaBiO<sub>3</sub>. Left — in cubic phase, right — in monoclinic phase.  $E_h$  is the energy of localised free level,  $E_f$  is the energy of the highest occupied Bi6sO2p<sub>σ\*</sub> orbital. The black and white circles with arrows denote electrons and holes, correspondingly, with opposite spin orientations. The occupied states of Bi6sO2p valence band are marked by grey. At the top, the local structure of octahedral complexes is shown. The [100] direction is equivalent to Bi-Bi direction. (b) The ground state of BaPbO<sub>3</sub>. The unoccupied band above the Fermi level  $E_F$  is shown. (c) The ground state of Ba<sub>1-x</sub>K<sub>x</sub>BiO<sub>3</sub>,  $x < 0.37$ . The splitting of free level  $E_h$  at spatial overlapping of BiL<sup>2</sup>O<sub>6</sub> octahedra is sketched.  $E_a$  is the activation energy  $E_a = E_h - E_f$ . (d) The ground state of Ba<sub>1-x</sub>K<sub>x</sub>BiO<sub>3</sub>,  $x > 0.37$ . The formation of unoccupied band above the Fermi level  $E_F$  at the percolation threshold reaching is sketched.

[17]. The optical gap  $E_g$  is the energy difference between the excited and ground states. In the excited state, BaBiO<sub>3</sub> has the local lattice of equivalent octahedra BiL<sup>1</sup>O<sub>6</sub> and possesses the non-compensated spin. Admittedly, it must have anti-ferromagnetic ordering, as the ground state in undoped cuprates La<sub>2</sub>CuO<sub>4</sub> and Nd<sub>2</sub>CuO<sub>4</sub>. Such optical excitation leads to the local dynamical lattice deformation observed in Raman spectra as a breathing mode  $\sim 570 \text{ cm}^{-1}$  of giant amplitude under resonant coinciding of photon energy of Ar<sup>+</sup> laser with  $E_g$  [19,20,49]. Using lasers with other quantum energies destroys this resonant effect and leads to abrupt decrease of breathing mode amplitude [20].

Thus, the scheme proposed accounts for the nature of the two energy gaps in BaBiO<sub>3</sub>. The activation energy  $E_a$  appears in transport measurements and is connected with coherent delocalisation of hole pairs owing to dynamic exchange BiL<sup>2</sup>O<sub>6</sub>  $\leftrightarrow$  BiO<sub>6</sub>. The optical gap is radically differs from a traditional gap in semiconductors.

It corresponds to energy difference between the excited and ground states.

## B. BaPbO<sub>3</sub>

In BaPbO<sub>3</sub>, each octahedron also has ten molecular orbitals, nine of which are filled and one, anti-bonding Pb6sO2p<sub>σ\*</sub>, is unoccupied as in octahedron BiL<sup>2</sup>O<sub>6</sub>, since lead has one electron less than bismuth. Thus, all the octahedral complexes represent the bound molecules PbL<sup>2</sup>O<sub>6</sub> with equal radii. At spatial overlapping of PbL<sup>2</sup>O<sub>6</sub> in crystal BaPbO<sub>3</sub>, wave functions of Pb6sO2p<sub>σ\*</sub> states become delocalised, unoccupied levels  $E_h$  of neighbouring octahedra split into a free carrier band, and, merging with the top of valence band consisting of initially filled Pb6sO2p<sub>σ\*</sub> orbitals, make the half filled conduction band (Fig. 9(b)). It is important to notice that unoccupied Bi(Pb)6sO2p<sub>σ\*</sub> orbitals in the case

of absence of spatial overlapping in BaBiO<sub>3</sub> behave as localised hole pairs, but transform to the conduction band at the spatial overlapping in BaPbO<sub>3</sub>. Because of this, BaBiO<sub>3</sub> appears to be a semiconductor of *p*-type, and BaPbO<sub>3</sub> — a semimetal of *n*-type. Since the radius of PbL<sup>2</sup>O<sub>6</sub> complex is slightly greater than that of BiL<sup>2</sup>O<sub>6</sub> complex, the Fermi level  $E_F$  in BaPbO<sub>3</sub>, according to expression (4), lies lower in comparison with  $E_f$  in BaBiO<sub>3</sub>, which agrees with results of photoelectron spectroscopy [50].

Thus, the lead valence state PbL<sup>2</sup>O<sub>6</sub> in BaPbO<sub>3</sub> is similar to the bismuth state in BiL<sup>2</sup>O<sub>6</sub> complexes in BaBiO<sub>3</sub>. According to Fig. 4, oxygen atoms in BaPbO<sub>3</sub> oscillate in the parabolic potential without any exchange between equal PbL<sup>2</sup>O<sub>6</sub> octahedra. Therefore, there is no charge pair transfer in semimetallic BaPbO<sub>3</sub> and the itinerant electrons behave as usual Fermi liquid.

### C. Ba<sub>1-x</sub>K<sub>x</sub>BiO<sub>3</sub>

The doping of BaBiO<sub>3</sub> by lead or potassium leads to decrease of integral structural lattice distortions and causes essential changes in both local crystal and electronic systems. Firstly, we discuss the changes in electronic structure of BKBO as a simpler case, and then will extend the obtained conclusions to the BPBO system.

Since K<sup>+</sup> ion has one valence electron instead of two of Ba<sup>2+</sup> ion, the substitution of each two Ba<sup>2+</sup> for two K<sup>+</sup> ions produces an additional unoccupied level or hole pair in a Bi6sO2p<sub>σ\*</sub> orbital and modifies the BiO<sub>6</sub> complex to the BiL<sup>2</sup>O<sub>6</sub>. As a result, the ratio of the numbers of BiL<sup>2</sup>O<sub>6</sub> and BiO<sub>6</sub> complexes changes from 1 : 1 in BaBiO<sub>3</sub> to (1 + *x*) : (1 - *x*) and equals 7 : 3 in Ba<sub>0.6</sub>K<sub>0.4</sub>BiO<sub>3</sub> and 3 : 1 in Ba<sub>0.5</sub>K<sub>0.5</sub>BiO<sub>3</sub>. The spatial overlapping of BiL<sup>2</sup>O<sub>6</sub> complexes appear, which, taking into account their small radii and rigid bonds, contracts the lattice. This leads to decrease and disappearance (at *x* > 0.37) of both static rotation- and breathing-type distortions. The lattice is forced to contract, despite the ionic radii of Ba<sup>2+</sup> and K<sup>+</sup> are practically equal.

Structural changes are accompanied by essential changes in physical properties of BKBO: at *x* ≈ 0.37 the phase transition insulator-metal occurs and the superconductivity arises that remains up to the dopant concentration *x* = 0.5 corresponding to the solubility limit of potassium in BaBiO<sub>3</sub>. The type of the temperature dependence of conductivity changes from semiconducting to metallic one, Hall coefficient changes its sign, and, in the normal state, BKBO compound with *x* > 0.37 behaves as a metal with *n*-type conductivity [25].

These changes are well described in the framework of the above scheme (Fig. 9 for BKBO). At the low dopant amount (*x* < 0.37), the contraction of the larger (soft) and the stretching of the smaller (rigid) octahedra bring, according to expression (4),  $E_h$  and  $E_f$  energies close together and the activation energy  $E_a = E_h - E_f$  de-

creases. As dopant concentration rises, the number of BiL<sup>2</sup>O<sub>6</sub> octahedra increases, and at *x* > 0.37, in the lattice arise the three-dimensional chains of spatially overlapped BiL<sup>2</sup>O<sub>6</sub> octahedral complexes [51], their unoccupied levels split and form the conductivity band, which is equivalent to the percolation threshold reaching that determines the insulator-metal phase transition. Here, the itinerant electrons show Fermi liquid behaviour with Fermi level  $E_F$  as in BaPbO<sub>3</sub>. However, in contrast to the picture in BaPbO<sub>3</sub>, in the BKBO structure there exist complexes BiO<sub>6</sub> through which itinerant electrons can not move because all the levels in these complexes are occupied. The movement of electrons occupying the upper Bi6sO2p<sub>σ\*</sub> orbital is possible only in pairing state at the dynamic exchange BiL<sup>2</sup>O<sub>6</sub> ↔ BiO<sub>6</sub>, since the unpairing costs energy consumption. But, in contrast to the case of BaBiO<sub>3</sub>, the static rotation- and breathing-type distortions of the octahedra disappear, their mean radii become approximately equal (and equal to half the lattice parameter), and the pair localisation energy approaches zero:  $E_a = E_h - E_f \rightarrow 0$  (Fig. 9(d)). In this case, the delocalised carrier pairs can freely move through the octahedral system that explains the appearance of superconductivity in BKBO (*x* > 0.37). This scheme of the local electronic structure is in full agreement with the picture of local oxygen vibration in double-well potential (see Figs.5,6,7).

The unpairing of electrons, as in BaBiO<sub>3</sub>, is possible under optical excitation and is manifested by a pseudo-gap observed in reflectivity spectra even in the metallic phase of BPBO-BKBO systems. For instance, in BKBO with *x* = 0.4 the pseudo-gap is about 0.5 eV [52] and about 0.6 eV [17] in BPBO with *x* = 0.25.

Our model suggests that in the metallic phase two carrier types are present: itinerant electrons and pairs of initially (in BaBiO<sub>3</sub>) localised carriers. The co-existence of the two carrier types was confirmed by experiments on investigation of conductivity, Hall effect, and thermoelectric power [17], as well as by photoemission spectra [23,50] and Raman spectra investigations [19,53]. These results are in a good agreement with observed zero-bias conductance [54]. The change in carriers behaviour from localised to itinerant at doping of BaBiO<sub>3</sub> by potassium was pointed to in x-ray absorption spectra analysis at the O *K* edge [33]. The analysis of EPR spectra [55,56] showed the presence of the localised carrier pairs, which also was confirmed by the observation of two-particle tunnelling in the normal-state of BKBO [54].

### D. BaPb<sub>1-x</sub>Bi<sub>x</sub>O<sub>3</sub>

Practically the same changes in electronic structure arise at the doping of BaBiO<sub>3</sub> by lead. The electronic structure of octahedral PbL<sup>2</sup>O<sub>6</sub> complex is entirely equivalent to that of BiL<sup>2</sup>O<sub>6</sub> complex. Unoccupied levels of overlapping octahedra in BaPbO<sub>3</sub> form the con-

duction band, as at overlapping of  $\text{Bi}\underline{\text{L}}^2\text{O}_6$  in BKBO. At the doping of  $\text{BaPbO}_3$  by bismuth ( $0 < x < 0.37$ ), the case is similar to BKBO ( $x > 0.37$ ). However, in BPBO the following combinations of neighbouring octahedra are possible:  $\text{Pb}\underline{\text{L}}^2\text{O}_6$ - $\text{Pb}\underline{\text{L}}^2\text{O}_6$ ,  $\text{Pb}\underline{\text{L}}^2\text{O}_6$ - $\text{Bi}\underline{\text{L}}^2\text{O}_6$ ,  $\text{Pb}\underline{\text{L}}^2\text{O}_6$ - $\text{BiO}_6$ ,  $\text{Bi}\underline{\text{L}}^2\text{O}_6$ - $\text{BiO}_6$ . This leads to different local shifts of  $E_h$  and  $E_f$  energies, depending on different octahedra neighbouring pairs. At the further increase of bismuth content, the number of filled  $\text{BiO}_6$  octahedra rises, the tilting and breathing distortions enlarge, the pair localisation energy raises, the spatial overlapping of unoccupied levels in  $\text{Pb}\underline{\text{L}}^2\text{O}_6$  octahedra disappears, which destroys the metallic type of conductivity and the system becomes a semiconductor with  $p$ -type conductivity.

Thus, superconductive properties of BPBO in our model are connected with dynamic exchange  $\text{Pb}\underline{\text{L}}^2\text{O}_6 \leftrightarrow \text{BiO}_6$ . Unfortunately, it is practically impossible to observe the double-well-potential oxygen vibrations for superconducting BPBO compositions ( $0 < x < 0.35$ ) by EXAFS study because of overlapping of  $\text{Pb } L_3$  and  $\text{Bi } L_3$  edges. Though an analysis of EXAFS spectra for these compounds is possible under elaborate treatment procedure [57], the precise enough values can be obtained only for interatomic distances, but not for amplitude factors. For this reason, we do not present the EXAFS data of BPBO ( $0 < x < 1$ ) in this paper.

### E. Photoemission spectra anomalies

The analysis of photoemission spectra has revealed a serious contradiction concerning the experimental observation of the splitting of the  $\text{Bi}4f(5/2, 7/2)$  spectral lines in superconducting compounds BKBO [24] at the absence of any peculiarities of those lines in parent  $\text{BaBiO}_3$  [23]. The contradiction consists in that though the analysis of x-ray diffraction and EXAFS data points to existence of two different Bi-O bonds in  $\text{BaBiO}_3$ , no splitting of  $\text{Bi}4f$  doublet lines was observed, which indicates the absence of considerable difference in bismuth valence states. The doping of  $\text{BaBiO}_3$  by potassium relieves the monoclinic distortion and equalises the Bi-O bond lengths up to  $a/2$ . However, the  $\text{Bi}4f$  spectral lines become broaden [23] and, at measurements on a high resolution spectrometer, even split [24], which, in contrast with simple cubic lattice in BKBO ( $x > 0.37$ ), points to existence of two different bismuth valence states.

The above scheme of local electronic structure completely resolves this issue. Indeed, in  $\text{BaBiO}_3$  the binding energies of the  $\text{Bi}4f$  core levels in different  $\text{Bi}\underline{\text{L}}^2\text{O}_6$  and  $\text{BiO}_6$  octahedra are almost equal and hence, the  $\text{Bi}4f$  doublet lines in photoemission spectra are unsplit (Fig. 10(a)). Contrary to that, in  $\text{Ba}_{0.6}\text{K}_{0.4}\text{BiO}_3$ , the binding energies of the  $\text{Bi}4f$  core levels in the different octahedra  $E'_1, E'_2$  and  $E_1, E_2$  differ on  $\Delta E = E_h - E_F \approx E_a$ , which causes the broadening (see curve  $x = 0.5$  in

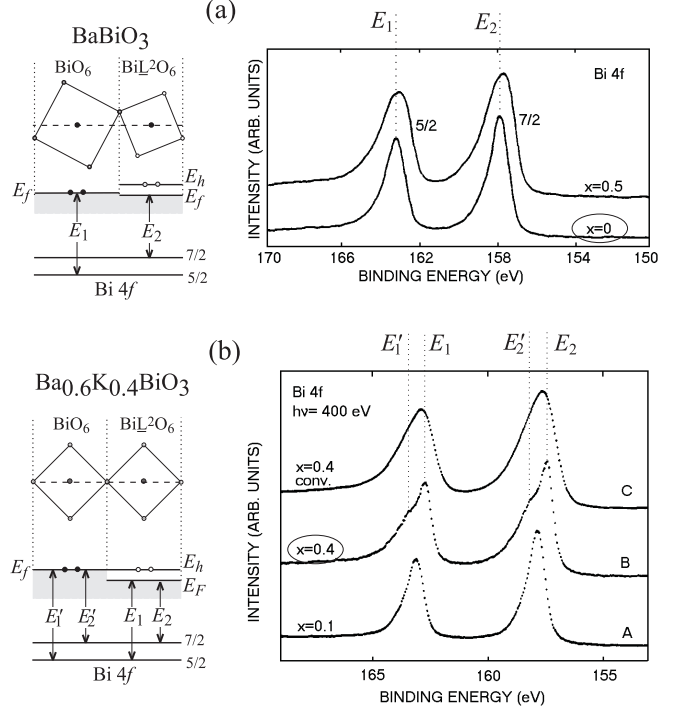


FIG. 10. Binding energies of  $\text{Bi}4f(5/2, 7/2)$  core levels in  $\text{Ba}_{1-x}\text{K}_x\text{BiO}_3$ : (a) for  $x = 0$ , right — experimental photoemission spectra from [23] with energy resolution  $\Delta E = 0.45$  eV; (b) for  $x = 0.4$ , right — experimental photoemission spectra from [24] with energy resolution  $\Delta E = 0.25$  eV. Curve C is the result of convolution of the curve B with Gaussian function with 0.75 eV width.

Fig. 10(a) from [23] and splitting (see curve  $x = 0.4$  in Fig. 10(b) from [24]) of the  $\text{Bi}4f$  doublet lines. The value of the splitting coincides well with our estimation of  $E_a = 0.48$  eV, and the ratio of intensities  $I$  of the core-level peaks corresponding to the binding energies in different octahedral complexes  $\text{BiO}_6$  and  $\text{Bi}\underline{\text{L}}^2\text{O}_6$  is in accordance with the relative content of these complexes in  $\text{Ba}_{0.6}\text{K}_{0.4}\text{BiO}_3$ :  $I(E'_1)/I(E_1) \simeq I(E'_2)/I(E_2) \simeq 3/7$ .

### V. ON POSSIBLE NATURE OF SUPERCONDUCTING STATE

Essentially anharmonic character of oxygen ion oscillations in soft rotation mode is the base of anharmonic model of the high temperature superconductivity [4]. It was shown that anharmonic coupling constant  $\lambda_s$  exceeds the constant in harmonic approach  $\lambda_{ph}$ :

$$\lambda_s/\lambda_{ph} \simeq J_s^2 d^2 \bar{\omega} / J_{ph}^2 \langle u^2 \rangle \omega_s \gg 1, \quad (5)$$

which explains high critical temperatures in cuprate HTSC compounds as well as in BPBO-BKBO systems. Here,  $d$  and  $\omega_s$  are the amplitude and frequency of oscillation in a double-well potential,  $\langle u^2 \rangle$  is the mean-square

displacement of the ions with the mean frequency  $\bar{\omega}$  in harmonic approach,  $J_{ph}^2$  and  $J_s^2$  are, respectively, the deformation potentials of harmonic and anharmonic oscillations averaged on the Fermi surface.

In that model, the oscillatory movement of oxygen ions in rotation mode with a large amplitude in the direction perpendicular to the Bi(Pb)-O bonds was considered. A considerable gain in value of the coupling constant in expression (5) is due to low frequency of soft rotation mode ( $\omega_s < \bar{\omega}$ ) and the excess of its amplitude over amplitude of harmonic oscillations ( $d^2 \gg \langle u^2 \rangle$ ).

Meanwhile, previous [12,27,28] as well as recent ([58] and references therein) electronic structure calculations showed that such a movement hardly affects the Bi-O bond lengths, keeping  $sp(\sigma)$  nearest-neighbour interaction nearly constant. Thus, despite the existence of double-well potential in rotation (tilting) mode, Meregalli and Savrasov [58] obtained very small anharmonic contribution to  $\lambda$ . Also, they assumed the breathing-type oxygen vibrations to be harmonic with small amplitude and high frequency and found too small  $\lambda \approx 0.3$  to explain high  $T_c$  in BKBO.

Our investigation firstly showed that in BKBO the double-well vibrations with strong deformation potential also exist along the Bi-O-Bi direction. Such vibrations have the breathing-like character and low frequency bounded by soft rotation mode. Thus, our results resolve the above issue and explain the reason for strong electron-phonon coupling in Bi-based oxides. Also, to these vibrations we can assign the low-frequency part, below 40 meV, of phonon density of states observed in neutron scattering for superconducting BKBO [59] and absent in calculations [58]. Besides, the anomalous phonon softening along [100] direction [60] becomes clear due to our observation of coherent breathing-like vibrations along [100] axis.

Hardy and Flocken [5] evaluated values of  $\lambda$ , using abstract model double-well potentials:

$$\lambda(T) = N(0) \sum_{kk'} \sum_{n' > n}^{FS} \frac{|\langle n | M_{kk'} | n' \rangle|^2}{E_{n'} - E_n} (f_n - f_{n'}), \quad (6)$$

where  $N(0)$  is the density of electron states at the Fermi level,  $M_{kk'}$  is the  $e$ -ph matrix element between electronic states  $|k\rangle$  and  $|k'\rangle$  on the Fermi surface,  $|n\rangle$  and  $|n'\rangle$  are the oscillatory states with energies  $E_n$  and  $E_{n'}$ ,  $f_n$  and  $f_{n'}$  are the thermal weighting factors;  $f_n = \exp(-E_n/kT) / \sum_{n'} \exp(-E_{n'}/kT)$ .

Given the oscillatory energies from our EXAFS-experiment, we have calculated  $\lambda$  in terms of arbitrary multiplicative constant which is proportional to  $N(0)$  and  $M_{kk'}$  (Fig. 11). Although “phonon” part of  $\lambda$  is the strongest for BaBiO<sub>3</sub>, this composition is not superconducting. On the one hand, because of pair localisation energy  $E_a$ . On the other, the rotation oscillations of rigid Bi $\underline{\text{L}}^2\text{O}_6$  octahedra and ordinary phonons (of stretching and bending types) differ in collective character of motion in BiO<sub>2</sub> planes. In BaBiO<sub>3</sub>, rigid Bi $\underline{\text{L}}^2\text{O}_6$  octahedra

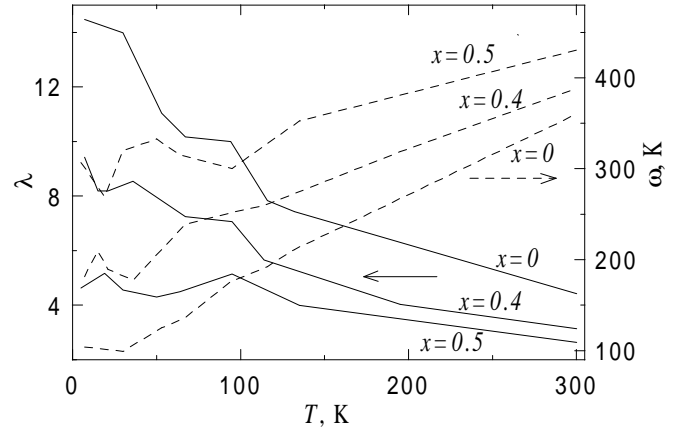


FIG. 11.  $\lambda$ 's in terms of arbitrary multiplicative constant (solid lines) and mean oscillatory frequencies (dashed lines) for Ba<sub>1-x</sub>K<sub>x</sub>BiO<sub>3</sub> with  $x = 0, 0.4, 0.5$  for double-well potentials obtained from EXAFS spectra treatment.

are separated by soft BiO<sub>6</sub> octahedra and are not spatially overlapped. The partial replacement of the larger soft octahedra by the smaller rigid ones at the potassium doping leads to decrease and disappearance of localisation energy  $E_a$  (Fig. 9(c,d)) and to spatial coherence of rotation oscillations with length of several lattice parameters, depending on the doping level  $x$ . For superconducting compositions,  $T_c$  means the temperature up to which  $\lambda$  is considerably decreased (Fig. 11) and/or the coherence in oscillations of neighbouring octahedra is thermally destroyed by ordinary phonons.

The ground state of BaBiO<sub>3</sub> can be considered as a bipolaronic state as well, and the movement of carrier pairs correlated with oxygen atoms oscillations at the dynamic exchange Bi $\underline{\text{L}}^2\text{O}_6 \leftrightarrow \text{BiO}_6$  evidences for possible application of bipolaron theory [61], which is supported by the small size of the pair (octahedron size) and by the existence of the pair state above  $T_c$ .

## VI. CONCLUSION

From the EXAFS investigation of BPBO-BKBO systems, the local crystal structure peculiarities connected with non-equivalence of Bi $\underline{\text{L}}^2\text{O}_6$ -BiO<sub>6</sub> octahedra were observed. It was found that oxygen vibrations are well described using double-well potentials, which leads to the strong electron-phonon coupling due to coherent modulation of Bi-O bond lengths with low frequency and causes correlated carrier pair movement with oxygen ions oscillations. The underlying relationship between the local crystal and local electronic structures was established that explains the full list of unusual properties of BPBO-BKBO systems: the existence of two energy gaps (transport  $E_a$  and optical  $E_g$ ) in BaBiO<sub>3</sub>; the mechanism of two-particle conductivity in BaBiO<sub>3</sub>; the co-

existence of two different carrier types; pseudo-gap observation in metallic compositions of BKBO and BPBO; the observation of localised pairs from EPR spectra; the observation of low-frequency ( $< 40$  meV) phonons; the nature of concentration and temperature phase transitions; the contradictions between local (Raman, and EXAFS) and integral structural methods for metallic BKBO; the anomalies of XPS spectra in  $\text{BaBiO}_3$  and BKBO. We observed the correlated movement of carrier pairs and low-frequency breathing-like oxygen octahedra vibrations, which corresponds to superconducting state. The model proposed combines some principal features of the real-space pairing [45], anharmonic models [4,5] and bipolaron theory [61] of high- $T_c$  superconductivity.

The likeness of rotation mode peculiarities of  $\text{BiO}_6$  octahedra and  $\text{CuO}_n$  complexes and the anomalies in temperature dependencies of Debye-Waller factors in cuprates [62] allow one to hope that similar model approach can be applied to the Cu-based superconductors.

## ACKNOWLEDGMENTS

We acknowledge LURE Program Committee for beam-time providing, Professors S. Benazeth and J. Purans for help during x-ray absorption measurements. We are also grateful to Professor A. P. Rusakov for high-quality BKBO samples and to Dr. A. V. Kuznetsov and Dr. A. A. Ivanov for helpful discussions. The work is supported by RFBR (Grant No. 99-02-17343) and Program "Superconductivity" (Grant No. 99010).

- 
- [1] A. W. Sleight, J. L. Gillson, and P. E. Bierstedt, *Solid State Commun.* **17**, 27 (1975).
  - [2] N. M. Plakida, *High-Temperature superconductivity* (Springer-Verlag, Berlin, 1995).
  - [3] J. P. Wignacourt, J. S. Swinnea, H. Steinfink, and J. B. Goodenough, *Appl. Phys. Lett.* **53**, 1753 (1988); G. H. Kwei, J. A. Goldstone, A. C. Lawson, Jr., J. D. Thompson, and A. Williams, *Phys. Rev. B* **39**, 7378 (1989).
  - [4] N. M. Plakida, V. L. Aksenov, and S. L. Drechsler, *Europhys Lett.* **4**, 1309 (1987).
  - [5] J. R. Hardy and J. W. Flocken, *Phys. Rev. Lett.* **60**, 2191 (1988).
  - [6] L. F. Mattheiss, E. M. Gyogry, and D. W. Jonson, Jr., *Phys. Rev. B* **37**, 3745 (1988).
  - [7] V. N. Stepankin, E. A. Protasov, A. V. Kuznetsov, and S. V. Zaitsev-Zotov, *Pis'ma Zh. Eksp. Theor. Fis.* **41**, 23 (1985), [*JETP Lett.* **41**, 27 (1985)].
  - [8] Z. Schlesinger, R. T. Collins, J. A. Calise, D. G. Hinks, A. W. Mitchell, Y. Zheng, B. Dabrowski, N. E. Bickers, and D. J. Scalapino, *Phys. Rev. B* **40**, 6862 (1989).
  - [9] Philip B. Allen, *Nature* **335**, 396 (1988).
  - [10] D. T. Marx, P. G. Radaelli, J. D. Jorgensen, R. L. Hitterman, D. G. Hinks, Shiyu Pei, and B. Dabrowski, *Phys. Rev. B* **46**, 1144 (1992).
  - [11] Shiyu Pei, J. D. Jorgensen, B. Dabrowski, D. G. Hinks, D. R. Richards, A. W. Mitchell, J. M. Newsam, S. K. Sinha, D. Vaknin, and A. J. Jacobson, *Phys. Rev. B* **41**, 4126 (1990).
  - [12] L. F. Mattheiss and D. R. Hamann, *Phys. Rev. B* **28**, 4227 (1983).
  - [13] D. E. Cox and A. W. Sleight, *Acta Crystallogr. B* **35**, 1 (1989).
  - [14] G. K. Wertheim, J. P. Remeika, and D. N. E. Buchanan, *Phys. Rev. B* **26**, 2120 (1982).
  - [15] Z. N. Akhtar, M. J. Akhtar, and C. R. A. Catlow, *J. Phys.: Condens. Matter* **5**, 2643 (1993).
  - [16] T. Hashimoto, H. Kawazoe and H. Shimamura, *Physica C* **223**, 131 (1994).
  - [17] S. Uchida, K. Kitazawa, and S. Tanaka, *Phase Transition* **8**, 95 (1987).
  - [18] S. Tajima, S. Uchida, A. Masaki, H. Takagi, K. Kitazawa, S. Tanaka, and A. Katsui, *Phys. Rev. B* **32**, 6302 (1985).
  - [19] S. Sugai, S. Uchida, K. Kitazawa, S. Tanaka, and A. Katsui, *Phys. Rev. Lett.* **55**, 426 (1985).
  - [20] S. Tajima, M. Yoshida, N. Koshizuka, H. Sato, and S. Uchida, *Phys. Rev. B* **46**, 1232 (1992).
  - [21] A. Balzarotti, A. P. Menushenkov, N. Motta, and J. Purans, *Solid State Commun.* **49**, 887 (1984).
  - [22] J. B. Boyce, F. G. Bridges, T. Claeson, T. H. Geballe, and J. M. Remeika, *Phys. Rev. B* **41**, 6306 (1990).
  - [23] M. Nagoshi, T. Suzuki, Y. Fukuda, K. Ueki, A. Tokiwa, M. Kikuchi, Y. Syono, and M. Tachiki, *J. Phys.: Condens. Matter* **4**, 5769 (1992).
  - [24] M. Qvarford, V. G. Nazin, A. A. Zakharov, M. N. Mikheeva, J. N. Anderson, M. K. J. Johansson, T. Rogelet, S. Söderholm, O. Tjernberg, H. Nylén, I. Lindau, R. Nyholm, U. O. Karlsson, S. N. Barilo, and S. V. Shiryaev, *Phys. Rev. B* **54**, 6700 (1996).
  - [25] H. Sato, T. Ido, S. Ushida, S. Tajima, M. Yoshida, K. Tanabe, and K. Tsubura and N. Miura, *Phys. Rev. B* **48**, 6617 (1993).
  - [26] T. Tani, T. Itoh, and S. Tanaka, *J. Phys. Soc. Jpn.* **49** Suppl. A, 309 (1980).
  - [27] N. Hamada, S. Massidda, A. J. Freeman, and J. Redinger, *Phys. Rev. B* **40**, 4442 (1989).
  - [28] M. Shirai, N. Suzuki, and K. Motizuki, *J. Phys.: Condens. Matter* **2**, 3553 (1990).
  - [29] Y. Koyama, S. I. Nakamura, and Y. Inoue, *Phys. Rev. B* **46**, 9186 (1992).
  - [30] Y. Yacoby, S. M. Heald, and E. A. Stern, *Solid State Commun.* **101**, 801 (1997).
  - [31] N. V. Anshukova, A. I. Golovashkin, V. S. Gorelik, L. I. Ivanova, and A. P. Rusakov, *J. Molecular Structure* **219**, 147 (1990).
  - [32] S. M. Heald, D. Di Marzio, M. Croft, M. S. Hegde, S. Li, and M. Greenblatt, *Phys. Rev. B* **40**, 8828 (1989).
  - [33] S. Salem-Sugui, Jr., E. E. Alp, S. M. Mini, M. Ramanathan, J. C. Campuzano, G. Jennings, M. Faiz, S. Pei, B. Dabrowski, Y. Zheng, D. R. Richards, and D. G. Hinks, *Phys. Rev. B* **43**, 5511 (1991).
  - [34] A. P. Menushenkov, S. Benazeth, J. Purans, A. Yu. Ig-

- natov, and K. V. Klementev, *Physica C* **277**, 257 (1997).
- [35] A. P. Menushenkov, in *Proc. of International Workshop on High Temperature Superconductivity — Ten Years after its Discovery*. (Ed.: K. B. Karg, S. M. Bose. Narosa Publishing House, Jaipur, India, 1996), p. 155; A. P. Menushenkov, *Nuclear Instruments & Methods in Physics Research A* **405**, 365 (1998).
- [36] J. Mustre de Leon, S. D. Conradson, I. Batistić, A. R. Bishop, I. D. Raistrick, M. C. Aronson, and F. H. Garzon, *Phys. Rev. B* **45**, 2447 (1992).
- [37] K. V. Klementev, in *Abstracts of Int. Conf. on X-ray Absorption Fine Structure XAFS-X* (August 10–14, Chicago, USA, 1998), p. 132, T5.2-14.
- [38] A. Yu. Ignatov, A. P. Menushenkov, and V. A. Chernov, *Physica C* **271**, 32 (1996).
- [39] N. V. Anshukova, A. I. Golovashkin, L. I. Ivanova, O. T. Malyuchkov, and A. P. Rusakov, *IEEE Trans. of Magn.* 1325 (1995).
- [40] M. Newville, P. Liviš, Y. Yacoby, J. J. Rehr, and E. A. Stern, *Phys. Rev. B* **47**, 14126 (1993).
- [41] P. A. Lee, P. H. Citrin, P. Eisenberger, and B. M. Kincaid, *Rev. Mod. Phys.* **53**, 769 (1981).
- [42] E. A. Stern, *Phys. Rev. B* **48**, 9825 (1993).
- [43] J. J. Rehr, J. Mustre de Leon, S. I. Zabinsky, and R. C. Albers, *J. Am. Chem. Soc.* **113**, 5135 (1991).
- [44] J. B. Boyce, F. G. Bridges, and T. Claeson, *Phys. Scripta* **42**, 71 (1992).
- [45] T. M. Rice and L. Sneddon, *Phys. Rev. Lett.* **47**, 689 (1981).
- [46] T. Claeson, J. B. Boyce, F. G. Bridges, T. H. Geballe, J. M. Remeika, and A. W. Sleight, *Physica C* **162–164**, 544 (1989).
- [47] S. Uchida, H. Hasegawa, K. Kitazawa, and S. Tanaka, *Physica C* **156**, 157 (1988).
- [48] Y. J. Uemura, B. J. Sternlieb, D. E. Cox, R. Kadono J. H. Brewer, J. R. Kempton, R. F. Kiefl, S. R. Kreitzman, G. M. Luke, P. Mulhern, T. Riseman, D. L. Williams, W. J. Kossler, X. H. Yu, C. E. Stronach, M. A. Subramanian, J. Gopalakrishnan, and A. W. Sleight, *Nature* **335**, 151 (1988).
- [49] S. Sugai, *Jpn. J. of Appl. Phys* **26** Suppl. 26-3, 1123 (1987).
- [50] H. Namatame, A. Fujimori, H. Torii, T. Uchida, Y. Nagata, and J. Akimitsu, *Phys. Rev. B* **50**, 13674 (1994).
- [51] For the simple 3D case (levels 0 and 1 allowable, percolation through the cubic cell side) the percolation threshold is well known  $p_c \approx 0.31$ . If the ground state represents the alternating cells of 0 and 1 states, our Monte Carlo calculations yield  $p_c \approx 0.15$ . If we additionally require that the percolating cluster must have at least one straight continuous chain in chosen direction, the percolation threshold  $p_c \approx 0.37$ .
- [52] S. H. Blanton, R. T. Collins, K. H. Kelleher, L. D. Rotter, Z. Schlesinger, D. G. Hinks, and Y. Zheng, *Phys. Rev. B* **47**, 996 (1993).
- [53] S. Sugai, *Phys. Rev. B* **47**, 3621 (1987).
- [54] E. S. Hellman and E. H. Hartford, Jr., *Phys. Rev. B* **52**, 6822 (1995).
- [55] S. K. Misra, S. I. Andronenko, R. R. Andronenko, and Larisa P. Mezentsseva, *Phys. Rev. B* **53**, 9442 (1996).
- [56] A. Yakubovskii, S. Gudenko, A. Rusakov, A. Golovashkin, and S. Verhovskii, *Physica C* **282–287**, 1929 (1997).
- [57] J. B. Boyce, F. G. Bridges, T. Claeson, T. H. Geballe, G. G. Li, and A. W. Sleight, *Phys. Rev. B* **44**, 6961 (1991).
- [58] V. Meregalli and S. Y. Savrasov, *Phys. Rev. B* **57**, 14453 (1998).
- [59] C. -K. Loong, P. Vashishta, R. K. Kalia, Wei Jin, M. H. Degani, D. G. Hinks, D. L. Price, J. D. Jorgensen, B. Dabrowski, A. W. Mitchell, D. R. Richards, and Y. Zheng, *Phys. Rev. B* **45**, 8052 (1992).
- [60] M. Braden, W. Reichardt, W. Schmidbauer, A. S. Ivanov, and A. Yu. Rumiantsev, *J. of Supercond.* **8**, 595 (1995).
- [61] A. S. Alexandrov and J. Ranninger, *Phys. Rev. B* **23**, 1796 (1981); A. S. Alexandrov, *Physica C* **158**, 337 (1989).
- [62] H. Maruyama, H. Kimura, A. Koizumu, H. Yamazaki, H. Maeda, and T. Ishii, in *X-Ray Absorption Fine Structure*. (Ed.: S. Samar Hasnain. Daresbury Laboratory, Warrington, UK, 1991), p. 370; H. Yamaguchi, H. Oyanagi, H. Ihara, Y. Kuwahara, and Y. Syono, *ibid*, p. 380.